Fundamentals of Forced Hydrolysis of Indium Hydroxide

Terry A. Ring#, Yoshiyuki Kudo*
*Department of Applied Chemistry
Science University of Tokyo
Tokyo, Japan
#Department of Chemical Engineering
University of Utah
Salt Lake City, Utah 84122

Abstract

During forced hydrolysis an acidified metal salt solution with its solution complexes is placed in a sealed test tube and heated at a specific rate to a high temperature <100°C. By heating the solution equilibria are altered, the hydroxide concentration is increased, and often a metal hydroxide is precipitated from solution as a narrow particle size distribution. This paper presents a theory that links solution complexation equilibria with a population balance model for precipitation predicting the particle size distribution. This model uses classical nucleation theory and growth rates by various rate limiting steps for the growth of the crystals. This theory is compared to forced hydrolysis experiments where dilute indium nitrate solutions, acidified with nitric acid, were placed in a water bath at 80°C for various periods of time. The experiments produced submicron cubic particles of Indium hydroxide. The experiments were monitored for temperature, pH, turbidity, and particle size distribution, all as a function of time for comparison with this model. Comparison of this experimental data with model calculation with the available solution complexation models for an acidified indium nitrate solution and various crystal growth models has been performed.

Introduction

Forced hydrolysis is a common way to produce metal hydroxides from an acidified metal salt solution. To induce precipitation, this solution, initially below its solubility limit and stable with respect to precipitation, is heated to an elevated temperature in either a forced convection oven or a water bath. Upon heating the solution, the concentration of OH- ion increases forcing the precipitation of a metal hydroxide. These metal hydroxides can be precipitated under controlled conditions as monodisperse colloids and as such are of interest for many applications including ceramic powders and pigments. Professor Matijevic[1] over his career has been able to produce monodisperse hydroxides of nearly all the metals in the periodic table. Over the years his work has been expanded by many researchers around the world.

In this work, we develop a model of forced hydrolysis which predicts both the particle size distribution of the precipitate and the concentration of all ions in solution as the precipitation takes place. This is done by performing a mass balance on the species in solution that precipitate and using these concentrations to predict the concentration of the other ions in solution assuming that the solution is in pseudo-equilibrium with respect to all other species. The results of this model are compared to the experimental system[2,3,4] where a

dilute $In(NO_3)_3$ solution acidified with HNO_3 is heated from room temperature to 80°C in a water bath causing the precipitation of cubic submicron $In(OH)_3(s)$. This experimental system was chosen because it is simple due to 1) a reduced suite of ionic complexes and 2) the precipitation of a crystal with a known geometry.

Experimental Methods

Experiments similar to those performed by Hamada, et. al.[5] giving submicron cubic crystalline $In(OH)_3$ particles were performed using a solution 3.96×10^{-4} M $In(NO_3)_3$ and 4.04×10^{-4} M HNO_3 , $pH_{initial} = 3.32$. A test tube with 50 ml of this solution was prepared and filtered through a 0.2 μm membrane filter and let stand for 24 hrs. at room temperature (22.0±0.5°C). Test tubes filled with this solution were then placed in a water bath (filled with a ethylene glycol solution to slow evaporation) at 80.0±0.1°C for various times. Test tubes were removed periodically, rapidly quenched to room temperature and measured as to their pH, light absorbance at λ=390nm and were then centrifuged at 700 G and washed repeatedly with distilled water using ultrasonic agitation[6] to resuspend the particle between centrifugation. The particle size distribution was measured taking samples on an Al stub for observation with a Cambridge Steroscan 240 Scanning Electron Microscope. The particle size distribution was measured by counting particles of different size on the SEM pictures. The arithmetic mean size and standard deviation were determined from the particle size distribution. A composite of all experimental data is presented in Figure 1. The measured pH (temperature compensated) decreases approximately 0.30±0.15 pH units after the temperature of the solution was raised. It is not known if the pH change is real. The change in pH for a 4.04×10^{-4}M HNO_3 solution heated in the same way was less than 0.05 pH units. The solution absorbance is near zero for nearly one hour then increases drastically initially and reaches a maximum at 90 min. As a result, we can presume that the particles are nucleated rather quickly (note, R* is ≈50Å for these values of S and T) and take time to grow to the a size that is sufficiently large to scatter light. The maximum value of absorbance is due to settling which decreases the particle number density as time progresses. The particle size increases with a decreasing rate and the standard deviation of the particle size distribution increases with growth time. This suggests[7] that n >0 in the growth function $\frac{dR}{dt} \alpha R^n$ of Table 4 given later in this paper. Please note that using chronomal analysis[8] of the average particle size as a function of time data, the Hamada group found that the growth was limited by a poly surface nucleation mechanism or n = 0

in the growth function $\frac{dR}{dt} \alpha R^n$ of Table 4. These experimental results for the particle size distributions may also be biased due to the sample preparation process in which centrifugation is used. Very small particles, <0.1μm in diameter, will not be present in the SEM pictures since they would have been discarded in the supernatant after the centrifugation steps.

Model Development

Mass balances are performed for the indium metal ions, M^{+m}, and OH^- ions. They are given by the generalized differential equations given below :

$$\frac{d[OH^-]}{dt} = \{\text{release of } OH^- \text{ from dissociation of } H_2O\}$$
$$-\{\text{Loss of } OH^- \text{ due to complexation with metal}\}$$
$$-\{\text{Loss of } OH^- \text{ due to nucleation}\}$$
$$-\{\text{Loss of } OH^- \text{ due to crystal growth}\} \quad (1)$$

$$\frac{d[M^{+m}]}{dt} = -\{\text{Loss of } M^{+m} \text{ due to complexation with various anions in solution}\}$$
$$-\{\text{Loss of } M^{+m} \text{ due to nucleation}\}$$
$$-\{\text{Loss of } M^{+m} \text{ due to crystal growth}\} \quad (2)$$

where [] symbolizes concentration. The initial conditions for these differential equations are:

$$[OH^-] = C_2, \text{ at } t = 0, [M^{+m}] = C_3 \text{ at } t = 0 \text{ and } [H^+] = C_1 \text{ at all time.}$$

All C_i values are constants. Since we are in dilute solution we will assume that activity and concentration are equivalent i.e. activity coefficients are 1.0. This is not totally accurate, however, to add activity coefficients, which are a function of the ionic strength, and their calculation to these two non-linear simultaneous differential equations would render them much more difficult to evaluate. Each of the terms of the above differential equations is discussed below after a discussion of the reactions that take place as an acidified metal salt solution is heated. To resolve these two coupled differential equations, a finite difference

technique was used. This finite difference technique was found to be stable if time steps less than 1 sec. were used.

Reactions in Solution

Metal complexation

Solution speciation reactions with anions A[= NO_3] :

$$iM^{+m} + jA^{-a} \underset{}{\overset{K_{Aij}}{\rightleftharpoons}} M_iA_j^{+(im-ja)} \qquad (3)$$

$$K_{Aij} = \frac{[M_iA_j]^{+(im-ja)}}{[M^{+m}]^i[A^{-a}]^j}$$

For this work, we will use the NO_3 complexes consisting of i:j of 1:1 and 1:2[9] given in Table 1. Solution speciation reactions with OH^- ions[10] also occur in solution :

$$iM^{+m} + jOH^- \underset{}{\overset{K_{OHij}}{\rightleftharpoons}} M_i(OH)_j^{+(im-j)} \qquad (4)$$

$$K_{OHij} = \frac{[M_i(OH)_j]^{+(im-j)}}{[M^{+m}]^i[OH^-]^j}$$

For this work, we will use Biedermann's [11,12] as well as Brown and Ellis[13] models of solution speciation of indium hydroxide complexes. Biedermann's model includes the complexes i:j , 1:1, 1:2, 2:2, 3:4. For these complexes, we have the equilibrium constant, K_{OHij}, and the ΔH_{OHij} of reaction[14] given in Table 2. The Brown and Ellis model includes the complexes i:j , 1:1, 1:2, 4:4 and 5:5. For these complexes, we have the equilibrium constant, K_{OHij}, and the ΔH_{OHij} of reaction[15] given in Table 3. Reaction kinetics between the 1:1 and the 2:2 complexes or dimerization have been studied by temperature jump experiments[16].

$$2\ In(OH)^{+2} \rightarrow In_2(OH)_2^{+4}$$

The forward rate constant for this reaction was found to be $4.1 \pm 0.4 \times 10^5\ M^{-1}\ sec^{-1}$. Thus this reaction is fast, occurring within a msec for the solution concentration typically used in forced hydrolysis. Other forward and backward reactions given in equation (4) have not been studied as to their reaction rates as evidence of the lack of information in the literature. In general, other solution speciation reactions can take place with other anions (or cations) B[=??] :

$$iM^{+m} + jB^{-b} \underset{}{\overset{K_{Bij}}{\rightleftharpoons}} M_iB_j^{+(im-jb)} \qquad (5)$$

$$K_{Bij} = \frac{[M_iB_j]^{+(im-jb)}}{[M^{+m}]^i[B^{-b}]^j}$$

However, in this experimental system, there are no other ions in solution for the metal to complex with but this is not always the case with forced hydrolysis of other metal hydroxides. When ammonium ions are in solution many metals are complexed e.g. Cu. Solution speciation reactions with anions A^{-a}, B^{-b} and OH^- lower the concentration of M^{+m} in solution.

Acid Dissociation

Acids present in solution dissociate. For nitric acid the reaction is :

$$H^+ + NO_3^- \underset{}{\overset{K_1}{\rightleftharpoons}} HNO_3 \qquad (6)$$

$$K_1 = \frac{[HNO_3]}{[H^+][NO_3^-]} = 10^{-1.44}\ @25°C \text{ and } 10^{-1.18}\ @70°C,\ \Delta H_{K_1} = 3.3\ Kcal/mole^{17}$$

Water Ionization

Water ionization equilibrium is also necessary to describe the experimental system:

$$H_2O \underset{}{\overset{K_w}{\rightleftharpoons}} H^+ + OH^- \qquad (7)$$

$K_w = [H^+][OH^-] = 10^{-13.999}$ @ 25°C and $10^{-12.422}$ @ 90°C[18,19]

In an acidified metal salt solution $[0H^-]$ is very low. For a solution with a fixed $[H^+]$, the $[0H^-]$ is increased by an increase in the temperature of the solution, since the value of K_w increases with temperature.

The predictions for $[H^+]$ and [OH-] for a 0.00078 M HNO_3 solution at various temperatures between 25°C and 100°C are given in Figure 2. Here we see that the $[OH^-] = K_w/[H+]$ increases from 10^{-11} M to 10^{-9} M while the [H+] and $[NO_3^-]$ are essentially unchanged. Experiments performed on this solution show a pH change of only 0.05 after temperature compensation. This change is similar to the noise level in these experiments. We will take advantage of this insignificant change in [H+] and $[NO_3^-]$ as temperature changes to simplify the necessary differential equations for the mass balance, i.e. no balance is necessary for H^+ or for NO_3^-.

Precipitation

The precipitation of a metal hydroxide is given by the following equilibrium :

$$M^{+m} + mOH^- \underset{}{\overset{K_{sp}}{\rightleftharpoons}} M(OH)_m(s) \qquad (8)$$

$K_{sp} = [M^{+m}][OH^-]^m$

where for Indium hydroxide K_{sp} is $10^{-36.9}$ M^3 at 25°C and 10^{-44} M^3 at 90°C (predicted value using ΔH_{sp}=24,789cal/mole[20]).

The supersaturation ratio, S, is given by :

$$S = \frac{[M^{+m}][OH^-]^m}{K_{sp}(T)} \qquad (9)$$

The rate of precipitation will dictate the loss rate of OH^- and In^{+3} ions due to the steps of nucleation and growth of the particles, discussed below.

Kinetics of Reactions and Precipitation

Release of OH^- due to ionization of H_2O

Rate of precipitation is controlled by the release rate of $[OH^-]$. We will make the assumption that the forward and reverse reactions responsible for the dissociation of H_2O are very fast (μsec.) compared to the rate at which heat can be transferred to the solution (min.) i.e. pseudo-equilibrium at each temperature. Thus the release rate of $[OH^-]$ is limited by the change in temperature of the solution[21]:

$$\frac{d[OH^-]}{dt} = \frac{d\left(\frac{K_w(T)}{[H+]_o}\right)}{dT}\frac{dT}{dt} = \frac{K_w(T)}{[H+]_o}\left(\frac{-\Delta H_w}{R_g T^2}\right)\frac{dT}{dt} \qquad (10)$$

assuming that the $[H^+]_o$ is fixed during the forced hydrolysis experiment. Note, R_g is the gas constant. As a result, the release of $[OH^-]$ is controlled by the heating rate, $\frac{dT}{dt}$, of the solution.

The temperature of the solution is altered by placing a test tube containing the solution into either a water bath or a forced convection oven. In either case, the test tube contents starts at a constant temperature, T_o, often room temperature and is immersed in a fluid with a constant temperature, T_∞, assumed to be an infinite heat reservoir. Heat is transferred to the solution by convection (natural or forced) through the walls of the test tube. We will make the assumption that the solution inside the test tube is all the same temperature and that the heat transfer is given by[22]:

$$V \rho C_p \frac{dT}{dt} = h_o (T_\infty - T) A \qquad (11)$$

where V is the volume, ρ is the density and C_p is the heat capacity of the solution in the test tube, A is the surface area of the test tube exposed to the heat reservoir and h_o is the overall heat transfer coefficient for both the inside and outside boundary layer, as well as, the heat

conduction for the glass wall of the test tube. The solution to this heat balance on the solution in the test tube is given by :

$$T = T_\infty + (T_o - T_\infty) \exp\left[-\left(\frac{h_o A}{V\rho C_p}\right) t\right] \qquad (12)$$

if we use the initial condition that the solution is at a constant temperature, T_o. Test tubes filled with the same volume of solution to be used in forced hydrolysis experiments have been subject to heating tests. The temperature in the test tube was measured with a thermocouple and plotted as a function of time. A plot of $(T_o-T_\infty)/(T_o-T_\infty)$ was plotted as a function of time and an exponential curve was used as a best fit (r^2=0.999). Analysis of the slope gives the parameter group $\left(\frac{h_o A}{V\rho C_p}\right)$ [= 0.775 min^{-1}] which is all that is needed to determine the temperature versus time curve for any initial, T_o, and bath, T_∞, temperature values.

The temperature change is rather slow in the water bath taking more than 5 minutes to reach 80°C. This equation gives a heating rate, $\frac{dT}{dt}$, for the solution in the test tube of :

$$\frac{dT}{dt} = -\left(\frac{h_o A}{V\rho C_p}\right) (T_o - T_\infty) \exp\left[-\left(\frac{h_o A}{V\rho C_p}\right) t\right] \qquad (13)$$

This heating rate can be used in the equation describing the release rate of [OH^-], equation (10), completing a theoretical description of the [OH^-] release rate. As a result of the heating rate, the concentration of OH^- can be calculated if losses due to nucleation and growth are accounted for as discussed below.

Loss of M^{+m} due to complexation with anions in solution

The heating rate will also release M^{+m} ions due to the altering of the solution speciation equilibria of the metal with A^{-a} and OH^- ions as given by[23] :

$$\frac{d[M^{+m}]}{dt} = \frac{dT}{dt}\left(\sum_i \frac{1}{i} \sum_j \frac{\left\{\frac{\Delta H_{OHij} + j\Delta H_w}{R_g T^2}\right\}}{\frac{1}{K_{OHij}[M^{+m}]^i[OH^-]^j} + \frac{1}{[M^{+m}]}} \right) +$$

$$\frac{dT}{dt}\left(\sum_i \frac{1}{i} \sum_j \frac{\{\frac{\Delta H_{Aij}}{R_g T^2}\}}{\frac{1}{K_{Aij}[M^{+m}]^i[A^{-a}]^j} + \frac{1}{[M^{+m}]}} \right) \qquad (14)$$

where $\frac{dT}{dt}$ is again the heating rate of the solution. This expression assumes that $[A^{-a}]$ is not dependent upon temperature which is the case if it is an independent ion added with the metal salt used in the initial formulation of the solution and not complexing anything but the metal. This is nearly the case with our experimental example (see figure legend for Figure 2). Other solution speciation, i.e. $[M_iB_j]$ can also be evaluated in the very same way giving and additional term like the M_iA_j term. For the Indium hydroxide system under investigation the equilibrium constants and the enthalpies are given in Table 1 and one of the Tables 2 to 3.

Loss of $[OH^-]$ and $[M^{+m}]$ due to Nucleation

With precipitation, we need a mass balance on $[OH^-]$ and $[M^{+m}]$ since they are changing with the formation of a metal hydroxide. The loss of is due to two processes ; nucleation and growth. For nucleation, we have :

$$\frac{d[OH^-]}{dt} = -\frac{3\rho}{M_w} J(S,T)\, R^*(S,T)^3 \qquad (15)$$

$$\frac{d[M^{+m}]}{dt} = -\frac{\rho}{M_w} J(S,T)\, R^*(S,T)^3 \qquad (16)$$

where ρ is the density and M_w is the molecule weight of the solid,

$J[=J_{max} \exp\{\frac{-32\,\gamma^3\,(\rho/M_w)^2}{(R_gT)^3\,(\ln S)^2}\}$[24]] is the nucleation rate[25,26,27] which is a function of time (i.e. S and T are functions of time) and $R^*[=\frac{12\,\gamma\,\rho/M_w}{3R_gT\,\ln S}]$ is the size of the critical nuclei[28], assuming nuclei and crystals are cubic. γ is the energy per unit area of the crystal in solution[29]. R* is also a function of time since S and T are functions of time.

Loss of $[OH^-]$ and $[M^{+m}]$ due to Crystal Growth

The crystals grow from the time they are nucleated until time t. The loss of $[OH^-]$ and $[M^{+m}]$ due to crystal growth is therefore given by :

$$\frac{d[OH^-]}{dt} = -\frac{3\rho}{Mw} \int J(S(t),T(t))\, dt \Big|_{t_{nucleated}} \int_{t_{nucleated}}^{t} R^2 \frac{d R}{dt} dt \qquad (17)$$

$$\frac{d[M^{+m}]}{dt} = -\frac{\rho}{M_w} \int J(S(t),T(t))\, dt \Big|_{t_{nucleated}} \int_{t_{nucleated}}^{t} R^2 \frac{d R}{dt} dt \qquad (18)$$

where $\frac{dR}{dt}$ is the growth rate of the crystal from the time it is nucleated until time, t. Generally, the growth rate has the form $\frac{dR}{dt} = C\, f(S)\, R^n$. Parameters in the various crystal growth rate models[30] are given in Table 4. All growth rates are a function of the saturation ratio, S, which is in turn a function of time.

Comparison of Model Calculations with Experiment

The utilization of this model allows the prediction of the values of $[In^{+3}]$, $[OH^-]$, S and all of the species of the type $In_i(OH^-)_j^{+(im-j)}$ or $In_i(NO_3^-)_j^{+(im-j)}$, assuming that $[NO_3^-]$ and [H+] are constant. These assumptions are some cause of errors < 0.4% as discussed in the legend of Figure 2, however, these assumptions drastically simplify the calculation and make the problem mathematically tractable. These result are highly dependent upon the growth model used for calculation and the parameters used in the growth rate theory e.g. the diffusion coefficient, D (10^{-5} cm/sec^2) and the parameters used for the interfacial energy (γ = 0.1 J/m^2)[31]. It should be pointed out that changes in the value of the interfacial energy drastically alters the model results. The reason for this is that the interfacial energy controls the critical free energy for surface nucleation through the value of the edge energy γ_e [= γ d][32] with units {erg/cm} and thus the rate of both mono and poly-surface nucleation. Changing the growth law alters the shape of the particle size distribution as it matures with time. Model results are given in Figure 3 for both the Biedermann, et. al. and the Brown and Ellis solution speciation models.

In Figure 3, we see the values of $[In^{+3}]$, $[OH^-]$ and S as a function of time as the solution is heated from 25° to 80°C. The OH^- concentration increases as the temperature increases.

This increase slows as nucleation and growth proceed. The In^{+3} concentration decreases monotonically as nucleation and growth proceeds. Since $S = \frac{[In^{+3}][OH^-]^3}{K_{sp}}$, we see that changes in $[In^{+3}]$ and [OH-] are reflected by the changes in S.

For the Biedermann model, S increases from ≈ 1 to ≈ 10,000 as the temperature increases and remains high > 1,000 for time >20 min. allowing both nucleation and growth to proceed for several hours at a very high supersaturation. Most of the particles are nucleated over a specific period of time (10 min. $>t_{nucleation}>$ 5 min.) giving a distribution of nucleii sizes but a lower level of nucleation continues over even a longer period of time. The particle size distributions in Figure 3D are plotted logarithmically to give a comparison of the results from the two models. However, plotting this same figure linearly provides a distribution function which is more like a Gaussian distribution but with some skewing to small particle sizes (see Figure 4B). For the Brown and Ellis model, S increases from ≈ 1 to ≈ 1,000,000 as the temperature increases and remains high > 100,000 for time >20 min. allowing both nucleation and growth to proceed for several hours at a very high supersaturation. Separate calculations show that the critical value of S is ≈1,000 thus nucleation will be insignificant for all values of S << 1,000 both before the peak in S and long after as the supersaturation is relieved by simultaneous nucleation and growth. The particle size distributions that result from the two models are shown in Figure 3D. These results show that prolonged nucleation as in the Biedermann speciation model give rise to a broad size distribution while shortened nucleation as in the Brown and Ellis speciation model gives rise to a narrow particle size distribution. Comparing the particle size distributions to those of the experiments, the Brown and Ellis model appears to give a better fit due to the shape of the particle size distribution.

Previous published results[33] used diffusion limited particle growth. The resulting number of particles per unit volume and the particle size as a function of time when compared to experimental values were not accurate (See Figure 4A). Essentially the number of particles per unit volume is too low and the particle size was to high to fit with the experimental data. To better tailor the model to experimental a slower growth model, e.g. poly surface nucleation model, is used (see Figure 4B). With the poly-surface nucleation growth law, the particle size distribution increases in width during subsequent growth since the growth law has a value of n >0 , n from Table 4. The prolonged nucleation observed in Figure 3D albeit at a lower level will also increase the width of the particle size distribution with time. This increase in the width of the particle size distribution and the more appropriate number densities of particles and more appropriate particle sizes suggests that the poly-surface

nucleation growth law coupled with the Brown and Ellis solution speciation model gives a reasonably good approximation to the experimental data. It should be pointed out that these model calculations were performed on a personal computer[34] but they took in some cases as long as 4 days to perform. This long computer run time is the reason that model calculations were not performed for comparison with long experimental durations.

The way this model has been formulated gives the ability to predict the changes in the concentration of solution species as the experiment proceeds. This is shown in Figures 5 and 6. Here we see for the Biedermann solution speciation model (Figure 5), that the various [OH^-] complexes initially increase in concentration due to an increase in [OH-] and then decrease in concentration as nucleation and growth proceeds. The concentration of [In^{+3}] and the $In_i(NO_3)_j$ complexes decrease monotonically. This situation is not in general different if the diffusion limited particle growth model is used. For the Brown and Ellis solution speciation model (Figure 6), we see that the various [OH^-] complexes initially increase in concentration due to an increase in [OH^-] and then decrease in concentration as nucleation and growth proceeds but this increase occurs over a longer time scale when compared to the Biedermann model, also observed in Figure 3. This prediction of the concentration of the various indium hydroxide complexes with time gives another method of model validation since some complexes are detectable with Raman Spectroscopy[35].

Conclusions

The hydrolysis of acidified $In(NO_3)_3$ solution has been studied experimentally. The result is a relatively narrow size distribution of submicron cubic $In(OH)_3$ crystals. A model of forced hydrolysis has been developed. This model accounts for the varying concentration of ions in solution as the precipitation proceeds and predicts the precipitated particle size distribution. It assumes that all chemical reactions in solution are fast compared to the change in solution temperature. The formalism of this model is a mass balance on both the metal, In^{+3}, and hydroxide, OH^-, ions in solution which allows calculation of the supersaturation ratio at any time which is the driving force for precipitation. Various crystal growth laws can be incorporated into the model. Comparison between model and experiment shows 1) that a poly-nuclear crystal growth law better explains the experimental data than the diffusion limited growth model used and

2) that the Brown and Ellis solution speciation model better explains the experimental data than the Biedermann, et. al. model.

Acknowledgement

The authors would like to thank the Professor S. Hamada and the Science University of Tokyo for providing funding for Dr. Yoshiyuki Kudo to work in the USA on this project. Electron microscopy was provided by Matt Nowell.

References

---

[1] Distinguished University Professor, Dept. Chemistry, Clarkson University, Potsdam, New York.

[2] Hamada, S. Kudo, Y., and Minagawa, K. Bull. Chem. Soc. Japan 63,102-107(1990).

[3] Yura, K., Fredrikson, K.C. and Matijevic, E., Colloids Surf. 50,281-293(1990).

[4] Yuar, E., and Matijevic, E., J. Colloid Interface Sci.in press.

[5] Hamada, S., Kudo, Y. and Minagawa,K., Bulletin of the Chemical Society of Japan, 63[1],102-107(1990).

[6] Branson 3200 ultrasonic bath.

[7] Dirksen,J.A. and Ring, T.A., Chem. Eng. Sci. 46(10),2389-2427(1991).

[8] Nielsen, A.E., Kinetics of Precipitation, Pergamon Press, Oxford, (1964).

[9] Ferguson, R.C., Doubud, P. and Tuck, D.G., J. Chem. Soc. (A) 1968, 1058.

[10] Some solution equilibria text books use metal hydryolysis equilibria of the type :

$$iM^{+m} + jH_2O \overset{K_{H2Oij}}{\blacktriangleleft\blacktriangleright} [M_i(OH)_j]^{im-j} + jH^+$$

To generate the $[M_i(OH)_j]^{im-j}$ ions. This type of equilibria can be converted to solution speciation reactions with the hydroxide ion of the type :

$$iM^{+m} + jOH^- \overset{K_{OHij}}{\blacktriangleleft\blacktriangleright} M_i(OH)_j^{+(im-j)}$$

by dividing the hydrolysis equilibium constant by the water dissociation equilibrium constant raised to the j power, as follows :

$$K_{OHij} = \frac{K_{OHij}}{K_w{}^j}$$

[11]Biedermann,G., Ark. Kemi.,9,277(1956). and Rec. Trav. Chim., 75,716(1956).

[12]Biedermann, G. and Ferri, D. Acta Chemica Scandinavica A 36,611-22(1982).

[13]Brown, P.L. and Ellis, J. J. Chem. Soc. Dalton Trans. 1911(1982)

[14]Smith, R.M. and Martel, A.E., "Critical Stability Constants, " Vol.4, Inorganic Complexes, Plenum Press, New York, 1976.

[15]Smith, R.M. and Martel, A.E., "Critical Stability Constants, " Vol.4, Inorganic Complexes, Plenum Press, New York, 1976.

[16]Eyring, E.M. and Owen, J.D., J. Phys. Chem.74[9],1825,1970.

[17]Silien, L.G. and Martel, A.E., "Stability Constants of Metal-ion Complexes," 2 nd. ed., Speciation publication, Chemical Society (Great Britain) , No.17, London Chemical Society, 1964.

[18]Silien, L.G. and Martel, A.E., "Stability Constants of Metal-ion Complexes," 2 nd. ed., Speciation publication, Chemical Society (Great Britain) , No.17, London Chemical Society, 1964.

[19]ΔH_w(cal/mole) = -2,6613 + 44.487*T(K) ≈ -13.34 Kcal/mole @ 25°C[19].

[20]determined from a Ksp vs 1/T fit of data from : Lacrois, S., Ann. Chim(France), 4,5(1949), Moelloer, T., J. Amer. Chem. Soc., 63,2625(1941) and Feitknecht, W. and Schindler, P. Pure Appl. Chem., 6,130(1963).

[21]This result was obtained by taking the log of the relationship $[OH^-] = \left(\frac{K_w(T)}{[H+]_o}\right)$ then taking the temperature derivative of both the right and left hand sides, where $[H+]_o$ is a constant. Using the relationship $\frac{d \ln K_w(T)}{dT} = \frac{-\Delta H}{RgT^2}$ and then expanding the term on the left handside $\frac{d \ln [OH^-]}{dT}$ to $\frac{[H+]_o}{K_w(T)} \frac{d[OH^-]}{dT}$ and rearranging.

[22]Bird.R.B., Stewart, W.E., Lightfoot, E.N., "Transport Phenomenon", John Wiley & Sons, New York, 1960.

[23]This first summation was obtained by rearranging the equilibria expression to :

$$\{M_iOH_j\}^{+(im-j)} = K_{OHij} \{M^{+m}\}^i \{OH^-\}^j$$

and taking the derivative with respect to temperature and noting that $\frac{d K_{OHij}}{dT} = K_{OHij} \left\{\frac{-\Delta H_{OHij}}{RgT^2}\right\}$

and that $\frac{d \{\{M_iOH_j\}^{+(im-j)}\}}{dT} = -i \frac{d\{\{M^{+m}\}\}}{dT}$ and then rearranging using expressions in ref. 19.

[24]Jmax for aqueous solution is either 10^{33} or 10^{30} #/cm^3/sec depending upon the theory used, see ref. 7.

[25]Becker, R. and Doring, W., Ann. Physik, 24, 719-752,(1935)

[26]Volmer, M. and Weber, A. , Z. Phys. Chem. 119,227,(1926)

[27]Nielsen, A.E., Kinetics of Precipitation, Pergamon Press, Oxford, (1964).

[28]Nielsen, A.E., Kinetics of Precipitation, Pergamon Press, Oxford, (1964).

[29]for data see, Nielsen, A,E. "Precipitates: Formation, Coprecipitation and Ageing" in Solution Equilibria and Chemistry, Pergamon Press, Oxford, (1994).

[30]Dirksen,J.A. and Ring, T.A., Chem. Eng. Sci. 46(10),2389-2427(1991).

[31]Nielsen, A,E. "Precipitates: Formation, Coprecipitation and Ageing" in Solution Equilibria and Chemistry, Pergamon Press, Oxford, (1994).

[32]ibid

[33]Kudo,Y. and Ring, T.A., Proceedings of the NATO Advanced Workshop on "Fine Particle Scinece and Technology from Micro to Nanoparticles" Acquafredda di Maratea, Italy July 15-21, 1995.

[34]MacIntosh II ci, 68030 CPU at 25mhz.

[35]Eyring, E.M. and Owen, J.D., J. Phys. Chem.74[9],1825,1970.

Tables and Figures

Table 1 Indium nitrate complexation reactions[1] - Equilibrium constants from R.C. Ferguson, P. Doubud and D.G. Tuck, J. Chem Soc. (A)1058(1968).

Reactions of the type $iM^{+m}+jNO_3^- \underset{\blacktriangleleft}{\overset{K_{NO3ij}}{\blacktriangleright}} M_i(NO_3)_j^{+(im-j)}$

i:j	$\log(K_{NO3ij})$ @25°C	ΔH (Kcal/mole)
1:1	-0.18	--
1:2	-0.3	--

Table 2 Indium hydroxide complexation reactions from Biedermann[2] - Equilibrium constants at Ionic Strength = 3 Molar $NaClO_4$. Equilibrium Constant data recalculated using the formula, $\log(K_{OHij}) = \log(K_{H2Oij}) - j \log (K_w)$[3]. Maximum n = 3.

Reactions of the type $iM^{+m} + jOH^- \underset{}{\overset{K_{OHij}}{\rightleftharpoons}} M_i(OH)_j^{+(im-j)}$

i:j	$\log(K_{OHij})$ @25°C	ΔH (Kcal/mole)
1:1	9.58	-8.2[4]
1:2	19.67	-13.0[5]
2:2	22.78	-16.0[6]
3:4	46.08	10.18*2=20.36[7]

Table 3 Indium complexation reactions from Brown and Ellis[10] - Equilibrium constants at 0.1 Molar KNO_3 Ionic Strength. Equilibrium Constant data recalculated using the formula, $\log(K_{OHij}) = \log(K_{H2Oij}) - j \log (K_w)$[11].

Reactions of the type $iM^{+m} + jOH^- \underset{}{\overset{K_{OHij}}{\rightleftharpoons}} M_i(OH)_j^{+(im-j)}$

i:j	$\log(K_{OHij})$ @25°C	ΔH (Kcal/mole)
1:1	9.69	-8.2[12]
1:2	18.64	-13.0[13]
4:4	48.66	--
5:5	19.00	--

Table 4 Crystal Growth Rate

$$dR/dt = C^*f(S)^*R^n$$

Growth Mechanism	C	f(S)	n	Ref
Diffusion Bulk	$\hat{V}DC_{eq}$	S-1	-1	14
Mono Surface Nucleation	$\beta_A D\ d^{-3}$	$\exp[\Delta G^*_s/k_BT]^{\S}$	2	15
Poly Surface Nucleation	$\frac{(Dd/3)}{(N_A C_{eq})^{2/3}}$	$(S-1)^{2/3}\exp[\Delta G^*_s/k_BT]^{\S}$	0	16
Screw Dislocation	$D_s n_{se}\beta/(y_o^2\rho)$	$S^2/S_1 \tanh(S_1/S)^{\S\S}$	0	17
Chemical Reaction	$\eta\hat{V}DC_{eq}$	S-1	-1	-

$^{\S}\Delta G_s^* = \beta_L^2 \gamma_e^2 d^2/(\beta_A k_B T \ln S)$

$^{\S\S}S_1 = (y_o/y_s)S$

$^{\S\S\S}\ln S = {}_T\int^T \Delta H_f/(RT^2)\, dT$

$\hat{V}$ is the molar volume, N_{Av} is Advogadro's number, C_{eq} is the equilibrium concentration, D is the diffusion coefficient, sub-s surface, η is the Damkohler Number, β_A is the area shape factor for surface nucleii, yo is the distance between steps, n_{se} is the equilibrium surface concentration, $\beta = 1-\sigma_s/S$ is one minus the maximum surface supersaturation divided by the solution supersaturation, γ_e is the edge energy of surface nucleii in units of energy per unit length, ρ is the density, $d = M_w/(\rho N_{Av})^{1/3}$, M_w is the molecular weight.

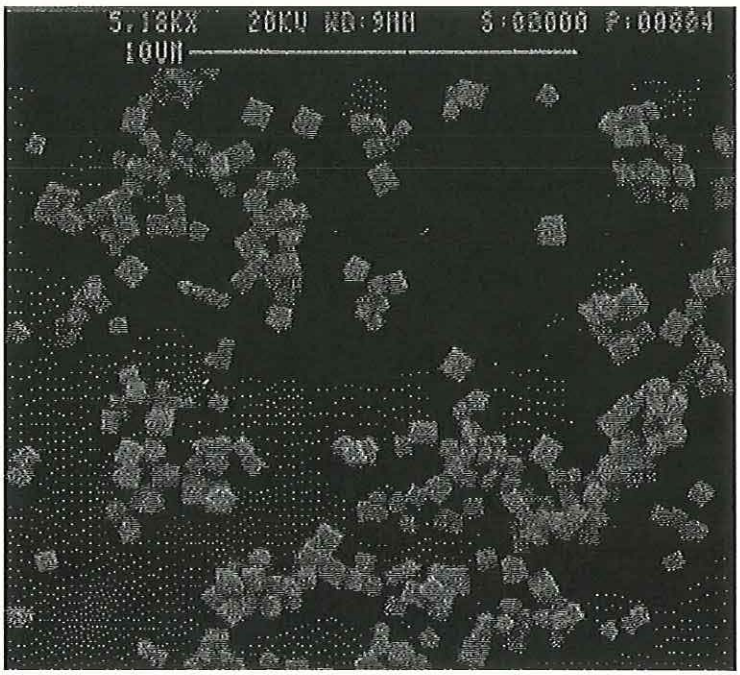

Blow-up Fig 1D

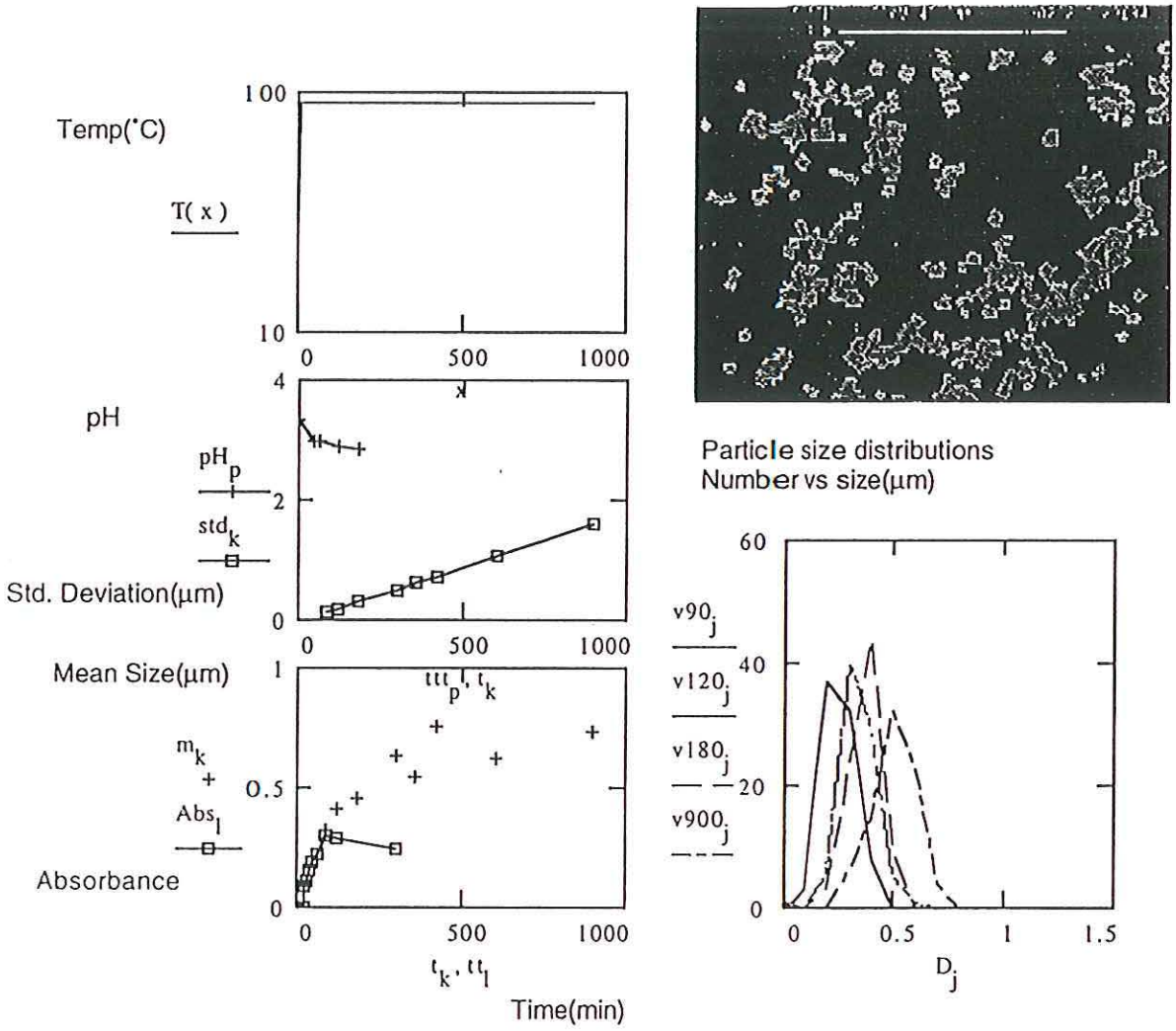

Figure 1. Plot of experimental data for an experiment performed with a 3.96×10^{-4}M $In(NO_3)_3$, 4.04×10^{-4}M HNO_3, pHi=3.32, A) temperature versus time, B) Mean size and Absorbance at λ=390nm (1 cm cell) versus time, C) Standard Deviation of particle size distributions versus time D) Scanning Electron Micrographs of particles produced at 4 hrs. (bar = 10 μm) and E) particle size distributions at various times v90= 90 min., v120= 120 min., etc., size = μm.

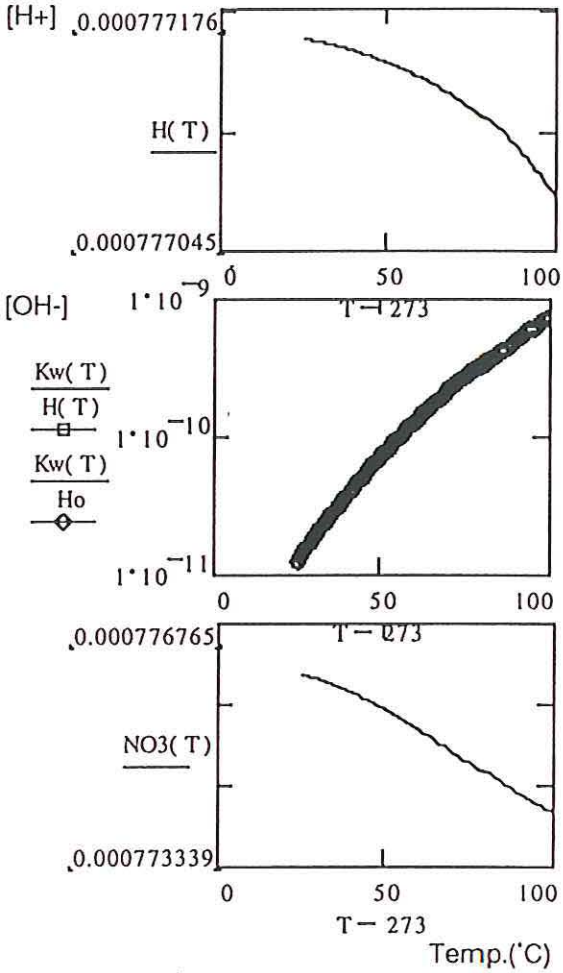

Figure 2. Prediction of $[NO_3^-]$, $[H^+]$ and $[OH^-]$ as a function of temperature between 25 and 100 °C. Please note that $[NO_3^-]$ and $[H^+]$ do not change by more than 0.4% and 0.04%, respectively, in this temperature range. Furthermore, if we assume that the $[H^+]$ is constant the error in $[OH^-]$ is less than 0.04%. This proves that NO_3^- complexes and $[H^+]$ do not vary significantly with temperature.

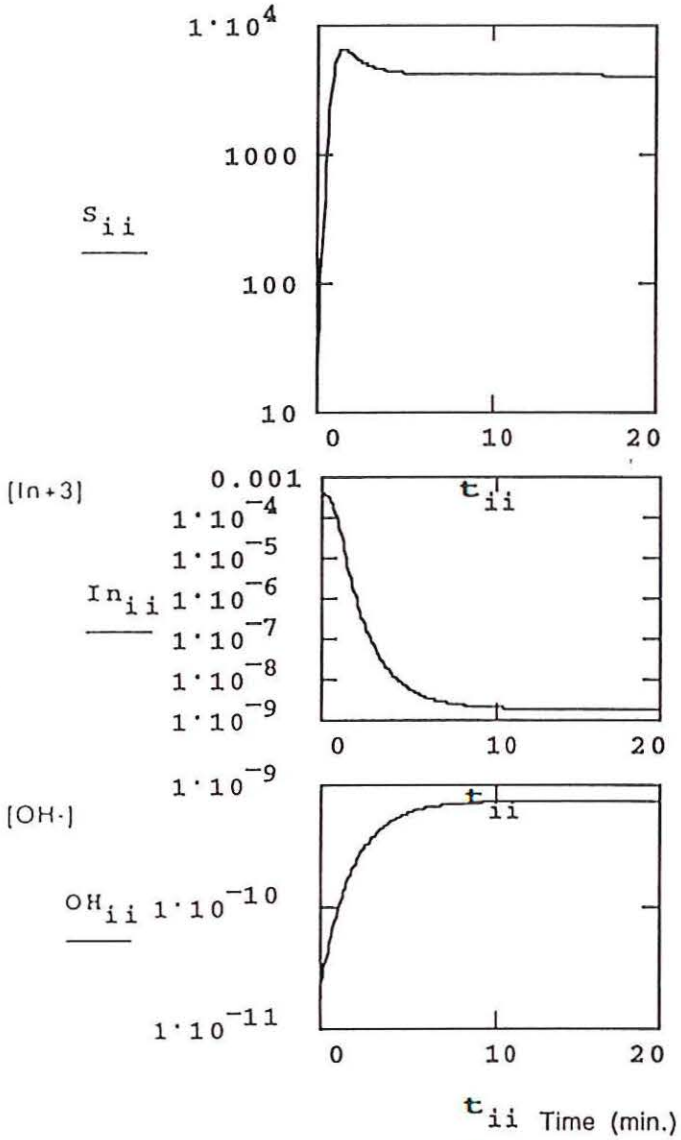

A,B,C Biedermann, et. al.

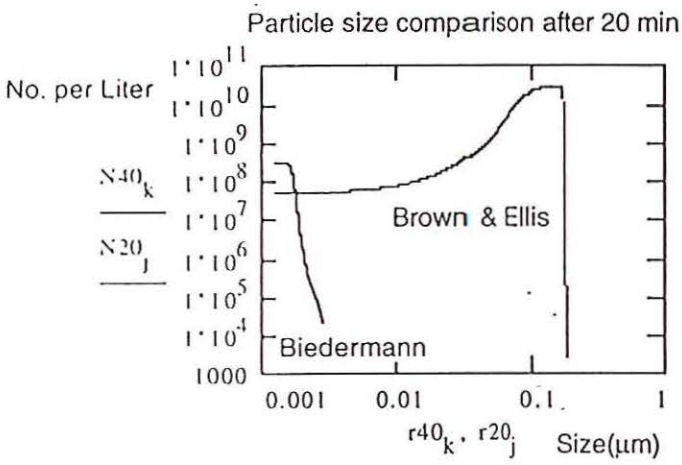

D

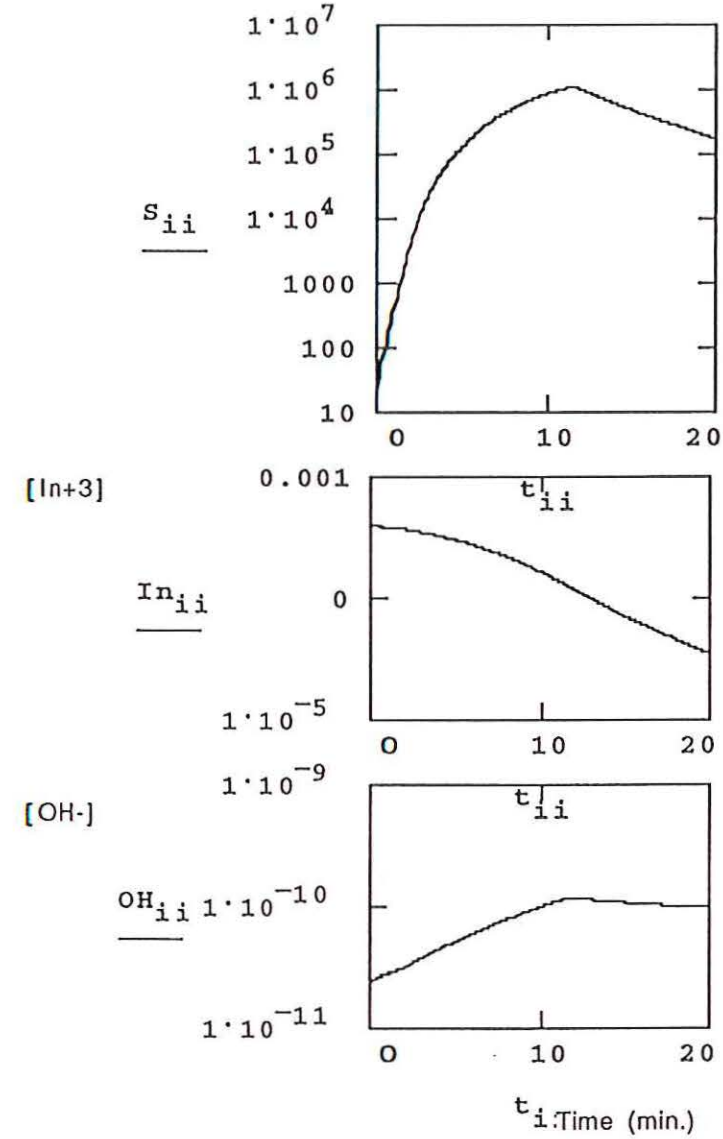

A,B,C Brown and Ellis

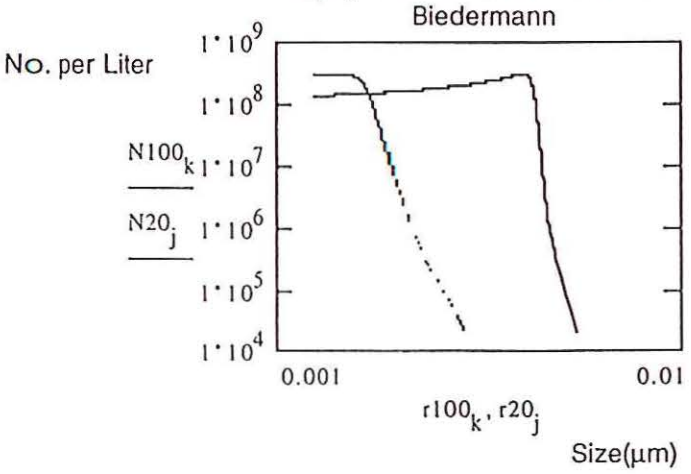

E

Figure 3 Model results for the Forced Hydrolysis of a solution $3.96x10^{-4}$M $In(NO_3)_3$, $4.04x10^{-4}$M HNO_3, pH_i=3.320. using homogeneous nucleation and poly surface nucleation limited growth. A) Saturation ratio versus time, B) $[In^{+3}]$ versus time, C) [OH-] versus time. On the left are the results using the Biedermann, et. al. solution speciation model and on the right are the results using the Brown and Ellis solution speciation model. D) Particle size distribution at 20 minutes for both solutions speciation models. E) Particle size distribution at 20 minutes ($N20_j$,$r20_j$) and 100 minutes ($N100_k$,$r100_k$) for Biedermann's solution speciation model.

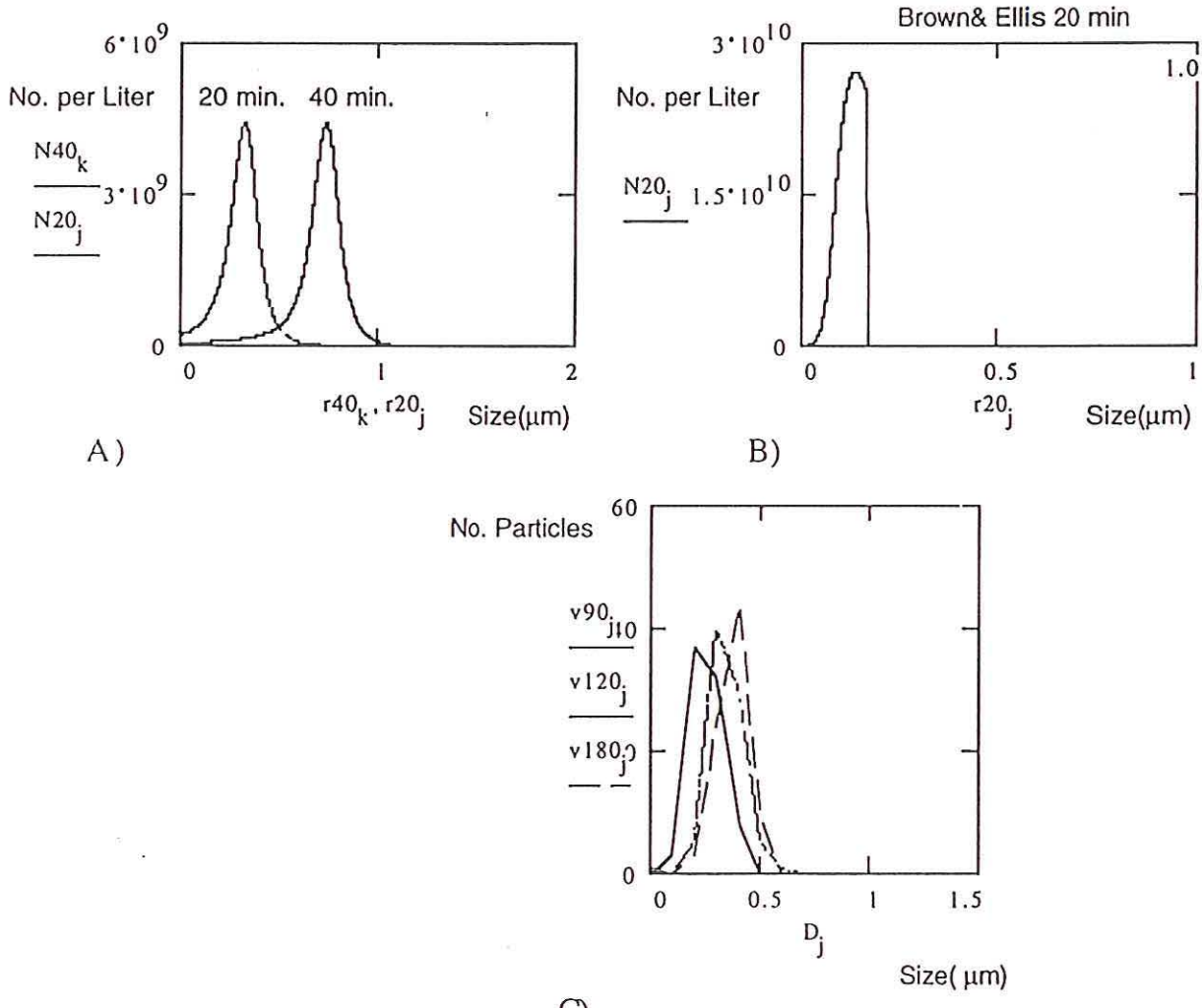

Figure 4. Comparison of particle size distributions produced by model with different Growth Laws. A) Diffusion limited Growth with Biedermann's solution speciation model, B) Poly-surface Nucleation limited Growth using the Brown and Ellis Solution speciation model (same plot as in Figure 3D but plotted linearly) and C) Experimental Data for the Forced Hydrolysis at 80°C of a solution $3.96x10^{-4}$M $In(NO_3)_3$, $4.04x10^{-4}$M HNO_3, pH_i=3.320.

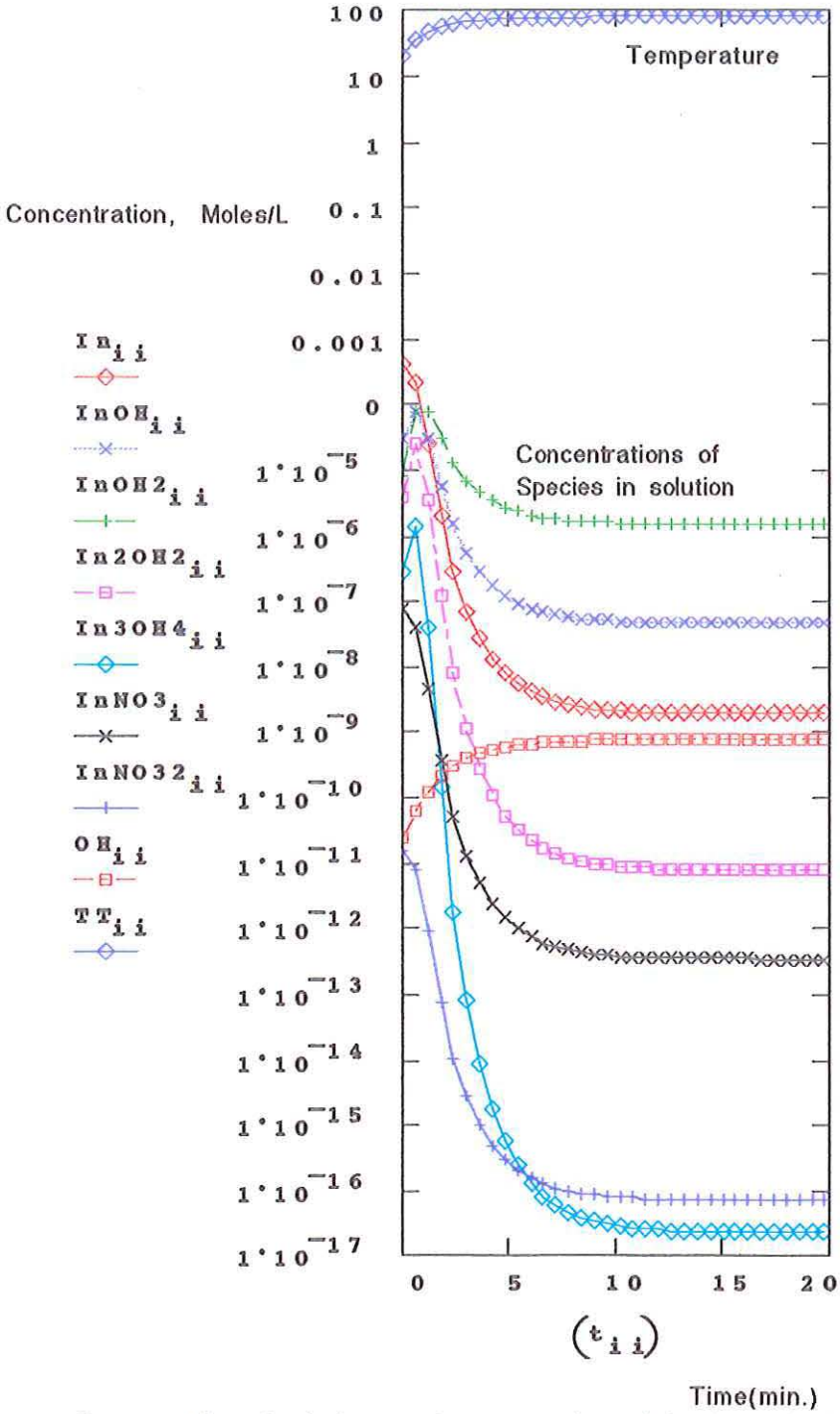

Figure 5. Concentration of solution species versus time of the forced hydrolysis of 3.96x10-4M In(NO3)3, 4.04x10-4M HNO3, pHi=3.32 using homogeneous nucleation and polynuclar growth and Biedermann's solution speciation model.

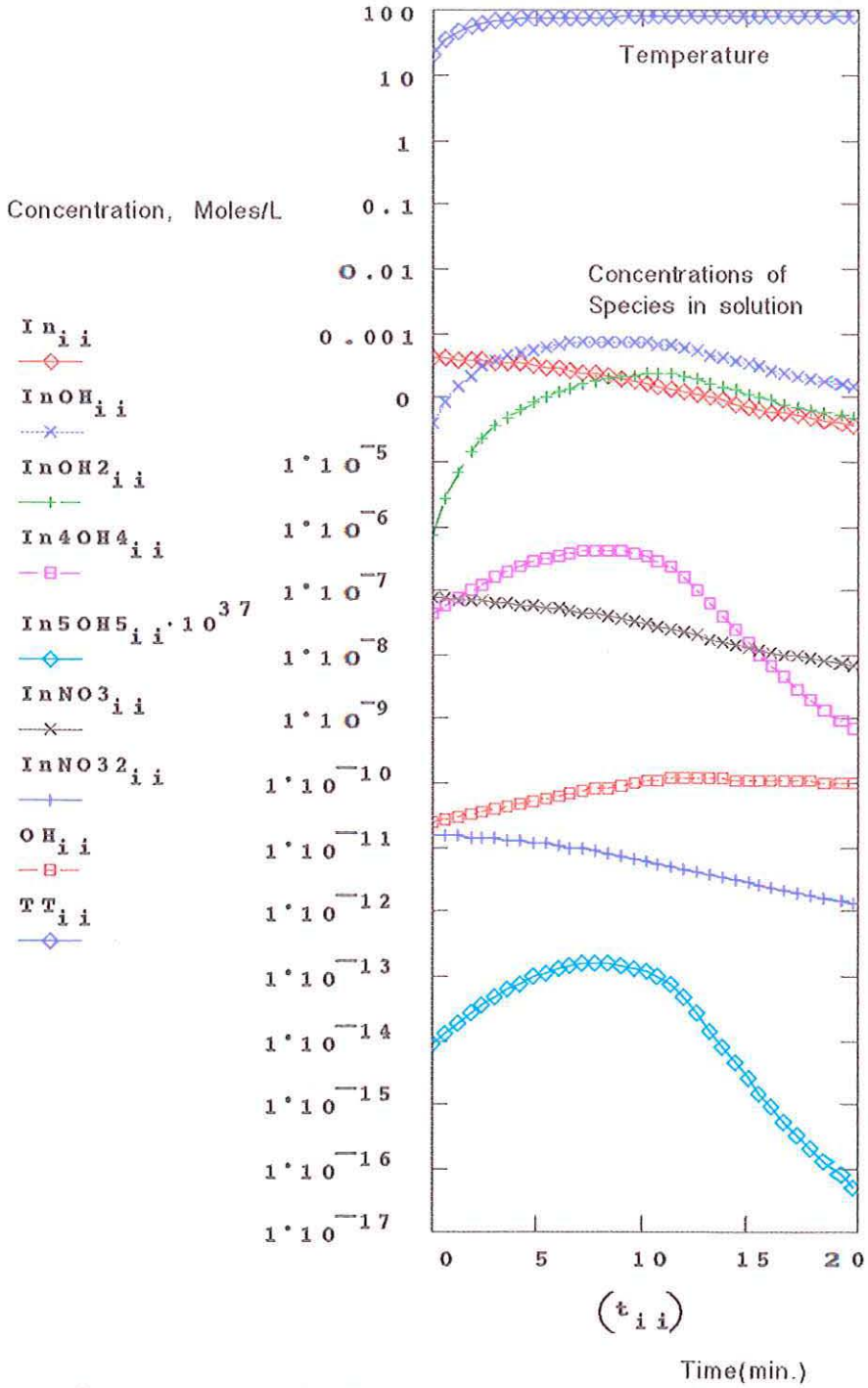

Figure 6. Concentration of solution species versus time of the forced hydrolysis of 3.96x10-4M In(NO3)3, 4.04x10-4M HNO3, pHi=3.32 using homogeneous nucleation and polynuclar growth and Brown and Ellis's solution speciation model.